Contents of this supplementary file

Supplementary Figures S1 to S8

Supplemental Figures S1–S8

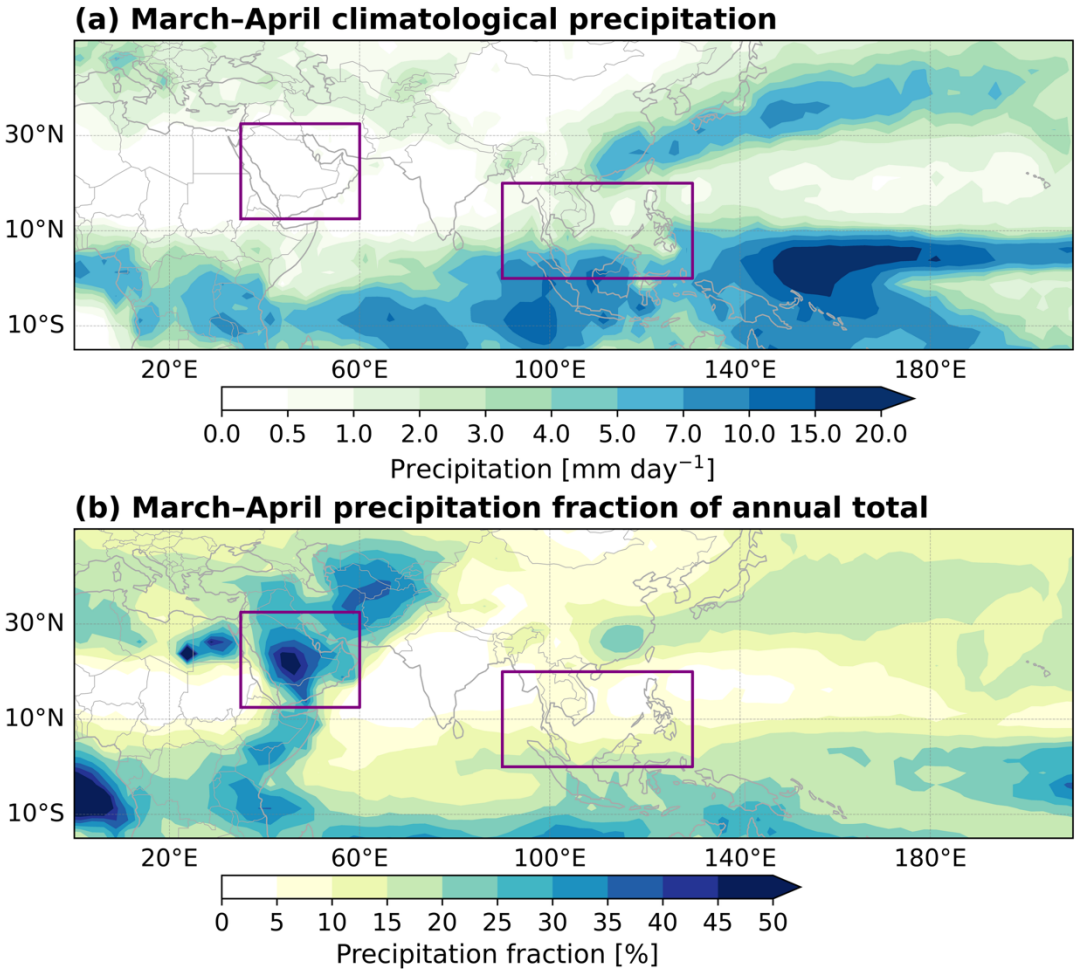

Supplementary Figure S1: Climatological March–April precipitation and its contribution to annual rainfall. (a) March–April mean precipitation climatology during 1979–2023. (b) March–April precipitation fraction of the annual total precipitation, expressed as a percentage. Purple boxes indicate the Arabian Peninsula (AP; 12.5°–32.5°N, 35°–60°E) and northern Southeast Asia (SEA; 0°–20°N, 90°–130°E) regions used to define the rainfall indices. Precipitation is from CMAP and is shown in mm day-1 in (a) and percentage of annual total in (b).

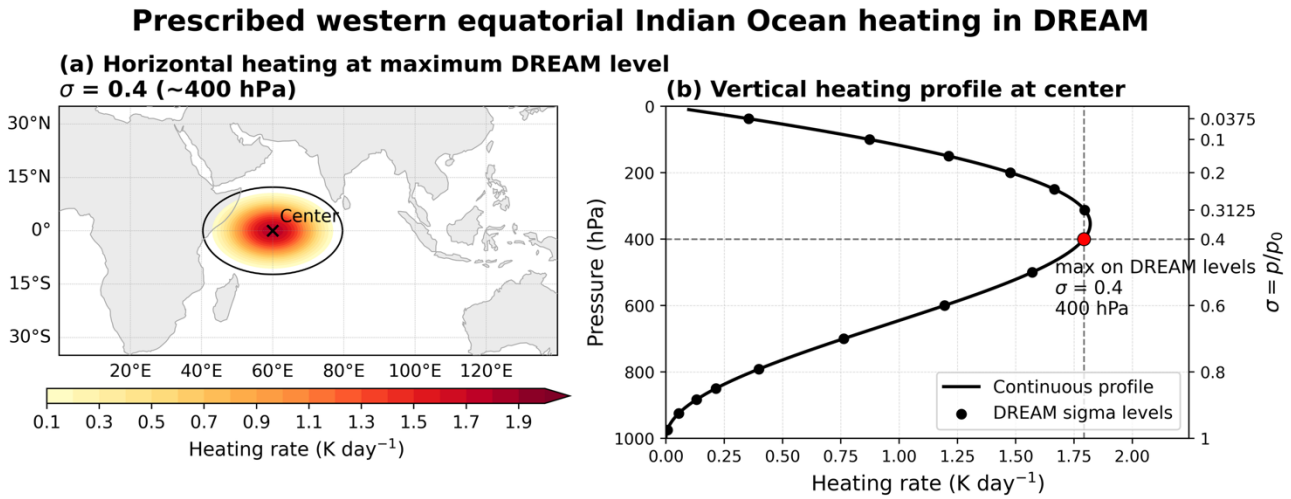

Supplementary Figure S2: Prescribed western equatorial Indian Ocean heating used in the DREAM experiments. (a) Horizontal distribution of the imposed heating at σ = 0.4 (~400 hPa), representative of the maximum-heating layer. The heating is centered at 60°E, 0°N and has an elliptical squared-cosine structure with horizontal radii of 20° longitude and 12.5° latitude. (b) Vertical heating profile at the heating center, defined as $Q(\sigma) = Q_0\pi(1-\sigma)\,sin[\pi(1-\sigma)]$, where Q_0 = 1 K day−1. The continuous profile peaks near σ = 0.35.

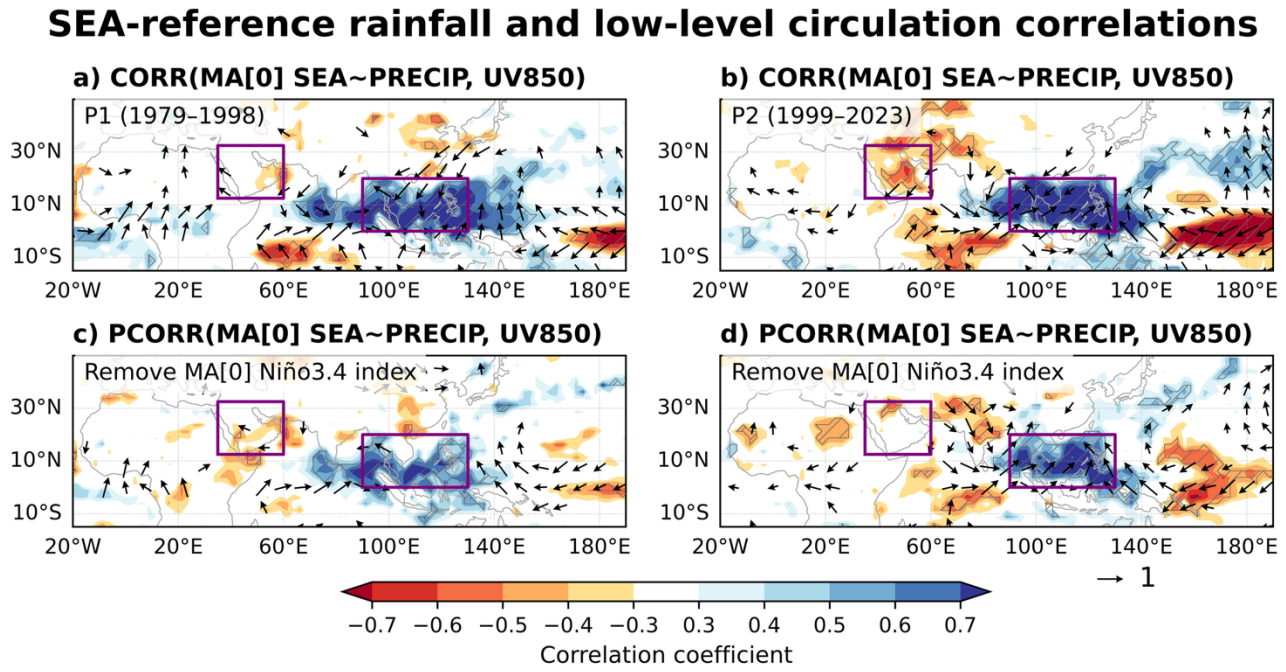

Supplementary Figure S3: Northern Southeast Asia-reference rainfall and low-level circulation correlations. Correlations of March–April rainfall anomalies (shading) and 850-hPa winds (vectors) with the northern Southeast Asia (SEA) rainfall index during (a) P1 (1979–1998) and (b) P2 (1999–2023). (c,d) As in (a,b), but after removing March–April Niño3.4 variability. Hatching denotes statistically significant rainfall correlations, and only significant wind vectors are shown. Purple boxes indicate the Arabian Peninsula (AP) and northern SEA regions. This figure provides a complementary SEA-reference perspective to Fig. 1, showing that the later-period AP–SEA rainfall and circulation linkage is weakened after removing Niño3.4 variability.

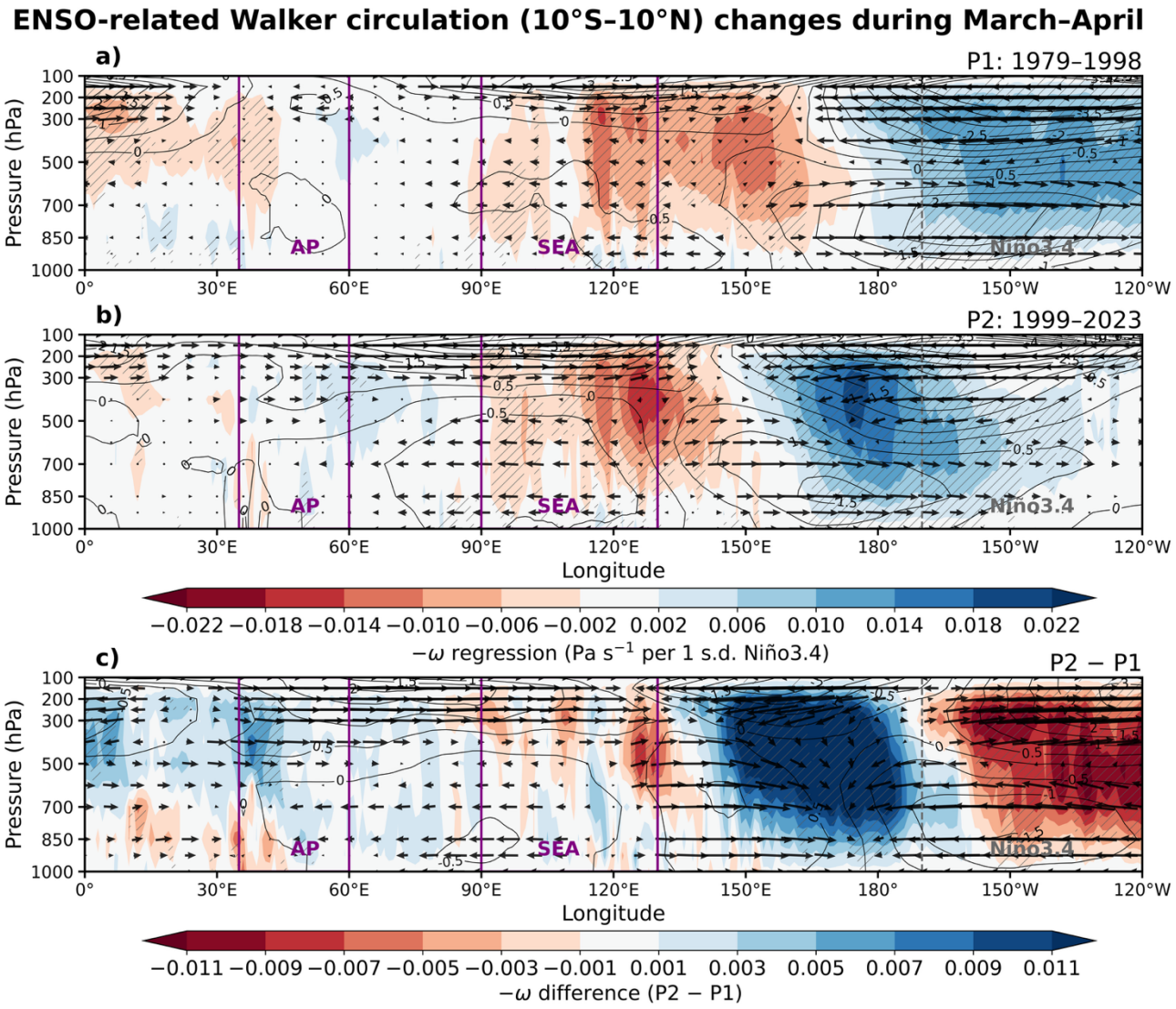

Supplementary Figure S4: ENSO-related Walker circulation changes during March–April. Longitude–pressure sections of March–April regression onto the standardized Niño3.4 index, averaged over 10°S–10°N. Shading denotes -ω regression anomalies, so positive values indicate anomalous ascent and negative values indicate anomalous subsidence. Vectors show the corresponding zonal–vertical divergent circulation, and contours show the zonal divergent wind component uχ. (a) P1 (1979–1998), (b) P2 (1999–2023), and (c) P2–P1 difference. Hatching indicates regions significant at the 95% confidence level. Purple vertical lines mark the AP, SEA, and Niño3.4 longitude ranges.

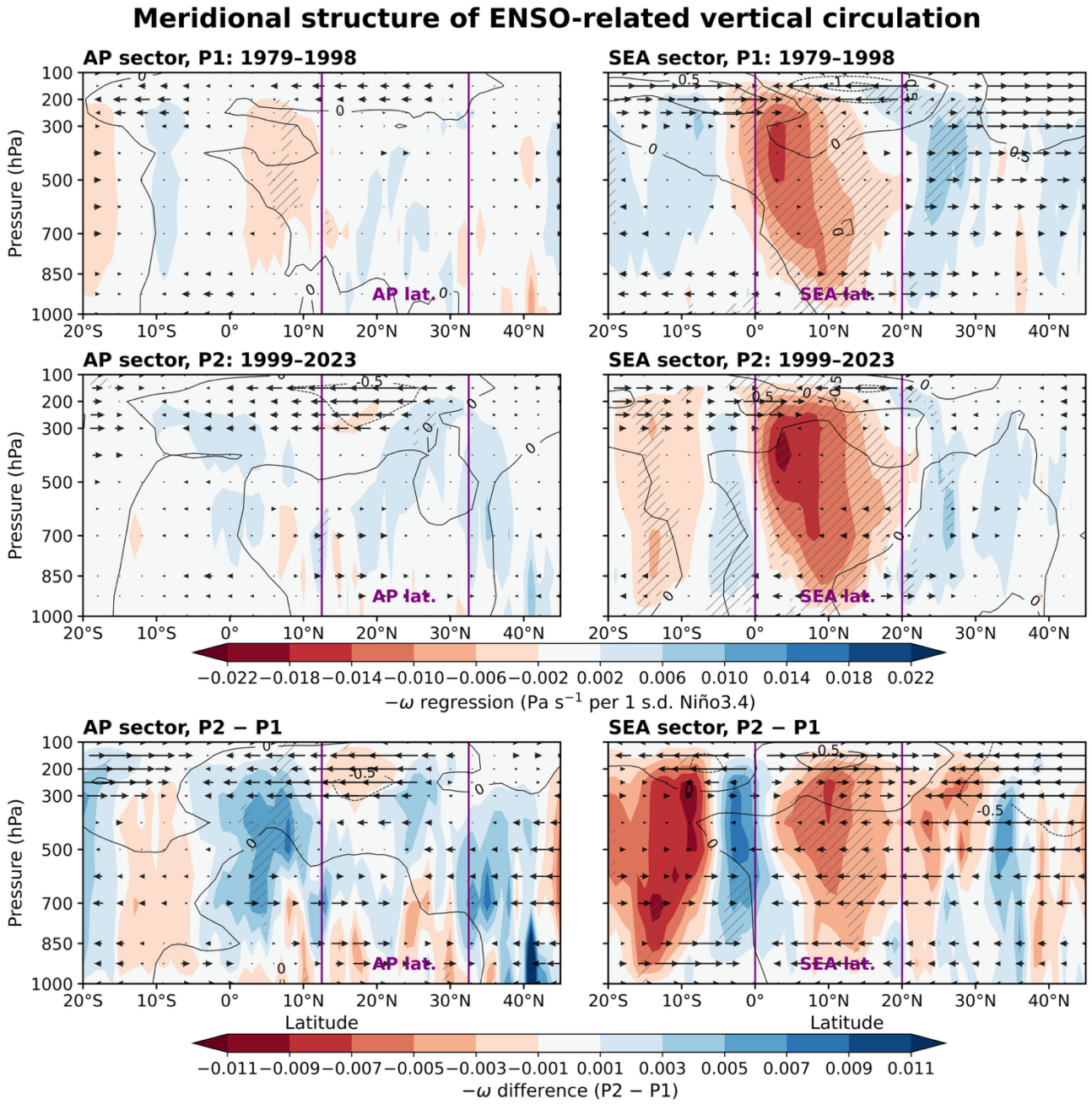

Supplementary Figure S5: Meridional structure of ENSO-related vertical circulation during March–April. Latitude–pressure sections of March–April regression onto the standardized Niño3.4 index. Shading denotes -ω regression anomalies, so positive values indicate anomalous ascent and negative values indicate anomalous subsidence. Vectors show the corresponding meridional–vertical divergent circulation, and contours show the meridional divergent wind component v_χ. The left column shows the AP sector averaged over 35°–60°E, and the right column shows the northern SEA sector averaged over 90°–130°E. The first two rows show P1 (1979–1998) and P2 (1999–2023), respectively; the bottom row shows the P2–P1 difference. Hatching indicates regions significant at the 95% confidence level. Purple vertical lines mark the AP and northern SEA latitude ranges used in the analysis.

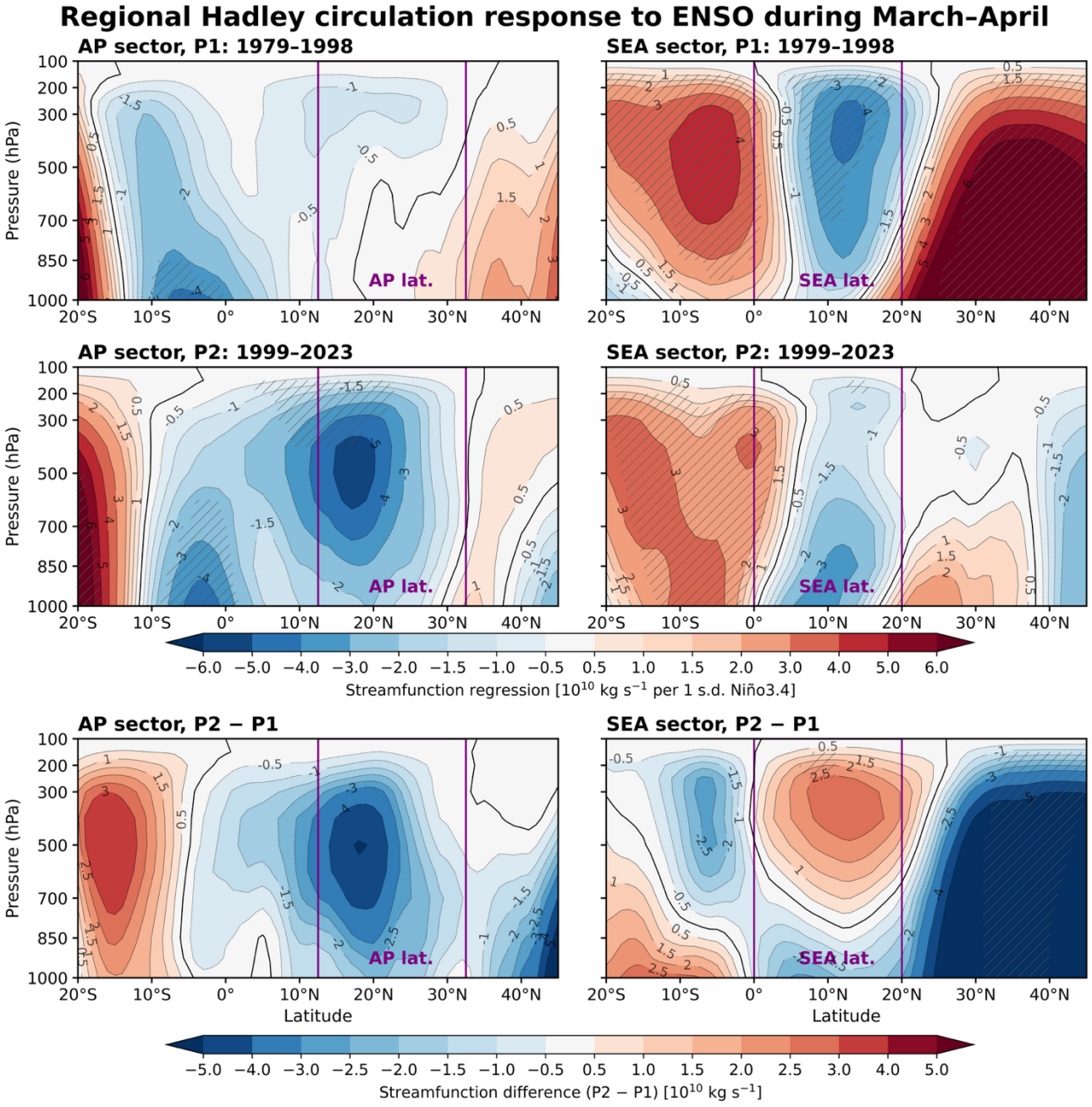

Supplementary Figure S6: Regional Hadley circulation response to ENSO during March–April. Latitude–pressure sections of March–April meridional mass streamfunction regression onto the standardized Niño3.4 index. The left column shows the AP sector averaged over 35°–60°E, and the right column shows the northern SEA sector averaged over 90°–130°E. The first two rows show P1 (1979–1998) and P2 (1999–2023), respectively; the bottom row shows the P2–P1 difference. Shading and contours denote the meridional mass streamfunction regression anomalies in units of 10^{10} kg s^{-1} per 1 s.d. Niño3.4 for P1 and P2, and the corresponding regression difference for P2–P1. Hatching indicates regions significant at the 90% confidence level. Purple vertical lines mark the AP and northern SEA latitude ranges used in the analysis.

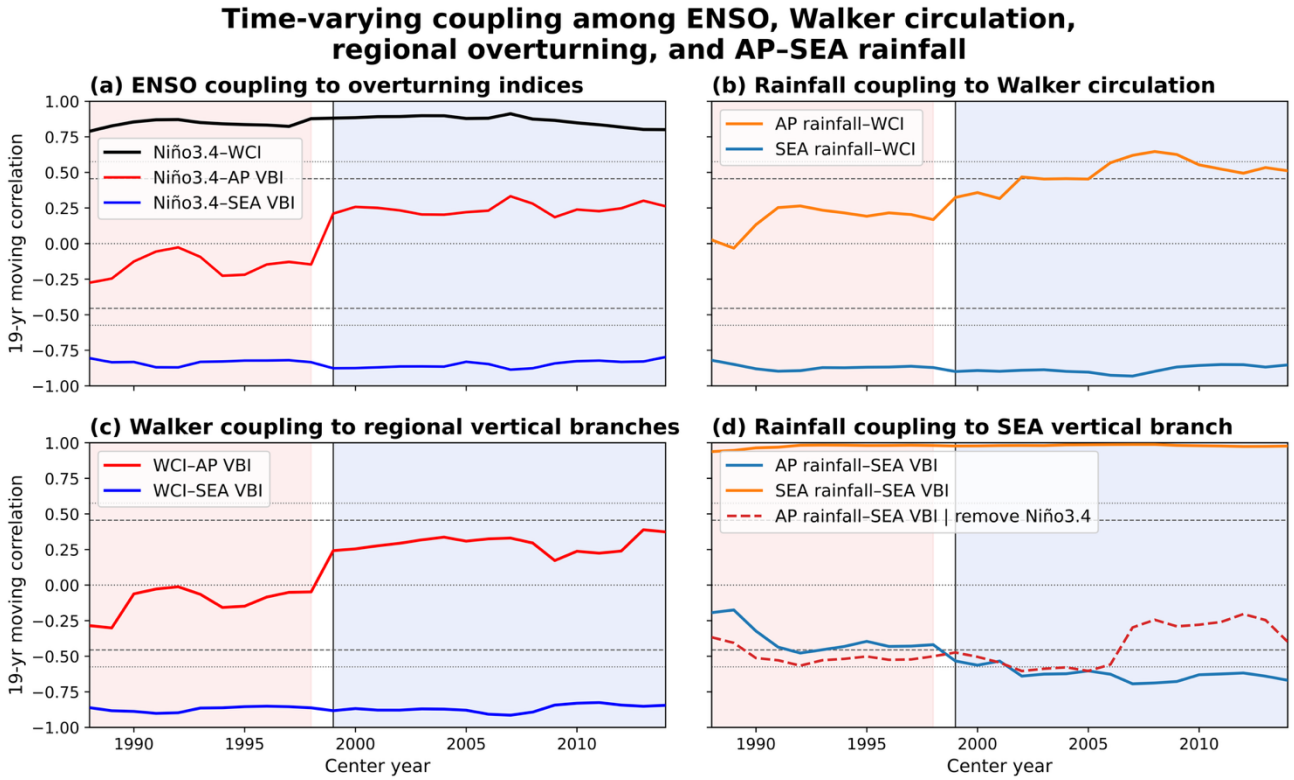

Supplementary Figure S7: Time-varying coupling among ENSO, Walker circulation, regional overturning, and AP–SEA rainfall. 19-year moving correlations among the March–April Niño3.4 index, Walker circulation index (WCI), regional vertical-branch indices (VBI), and rainfall indices over the Arabian Peninsula (AP) and northern Southeast Asia (SEA). The WCI is defined from the sea-level pressure anomaly difference between the eastern and western tropical Pacific, with the sign reversed so that positive values correspond to an El Niño-like weakening of the Pacific Walker pressure gradient. The VBI is defined using 700–300-hPa layer-mean -ω, so positive values indicate stronger upward motion. (a) Correlations of Niño3.4 with WCI, AP VBI, and SEA VBI. (b) Correlations of AP and SEA rainfall with WCI. (c) Correlations of WCI with AP and SEA VBI. (d) Correlations of AP and SEA rainfall with SEA VBI; the dashed red line shows the AP rainfall–SEA VBI relationship after removing Niño3.4 variability. Dashed and dotted horizontal lines denote the 95% and 99% significance levels, respectively. Red and blue shading mark moving-correlation windows centered in P1 and P2, respectively.

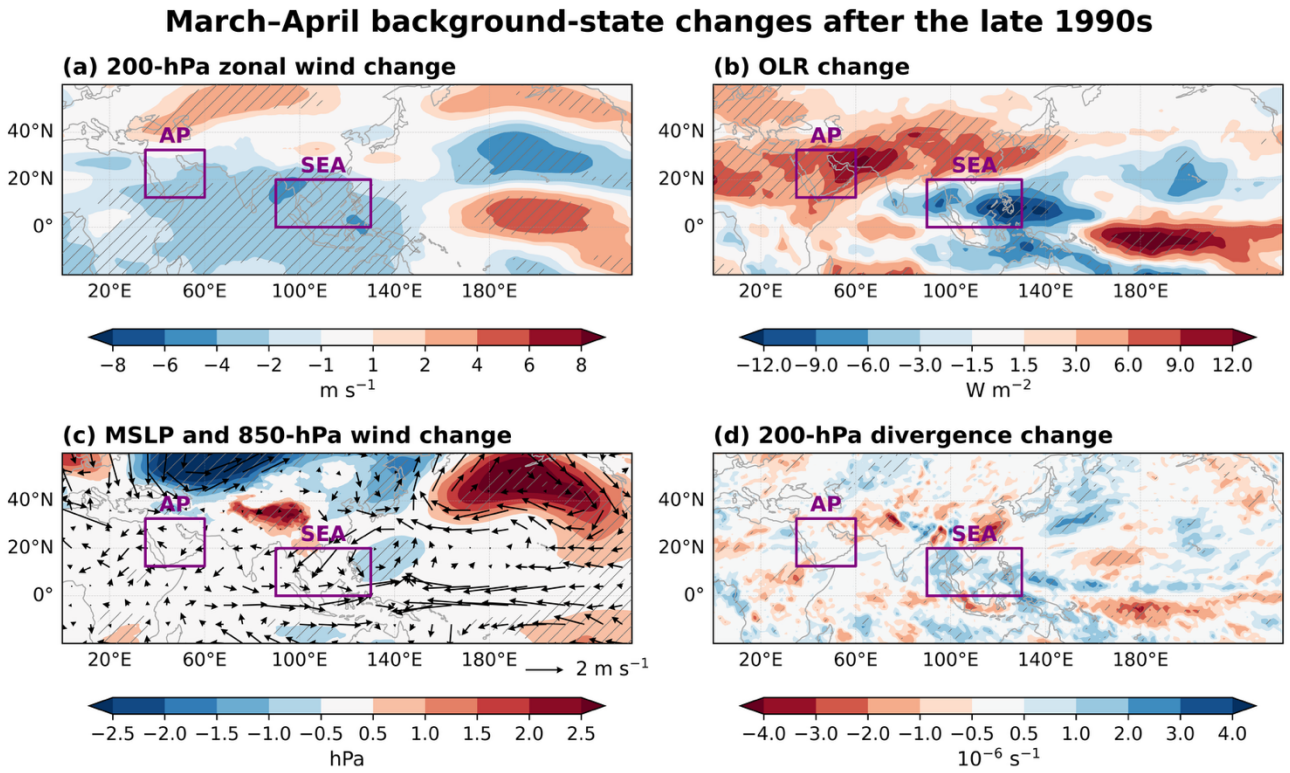

Supplementary Figure S8: March–April background-state changes after the late 1990s. P2–P1 differences in March–April mean background state between P2 (1999–2023) and P1 (1979–1998). (a) Difference in 200-hPa zonal wind. (b) Difference in outgoing longwave radiation (OLR). (c) Difference in mean sea-level pressure, with vectors showing the corresponding 850-hPa wind changes. (d) Difference in 200-hPa horizontal divergence. Hatching indicates regions significant at the 95% confidence level, and only significant wind vectors are shown in (c). Purple boxes indicate the Arabian Peninsula (AP) and northern Southeast Asia (SEA) regions. These fields show the modified March–April basic-state environment in which ENSO-related anomalies developed after the late 1990s.